**Atmospheric
Measurement
Techniques**

Diode laser-based cavity ring-down instrument for NO_3, N_2O_5, NO, NO_2 and O_3 from aircraft

N. L. Wagner[1,2], W. P. Dubé[1,2], R. A. Washenfelder[1,2], C. J. Young[1,2], I. B. Pollack[1,2], T. B. Ryerson[1], and S. S. Brown[1]

[1]NOAA Earth System Research Laboratory, R/CSD7, 325 Broadway, Boulder, CO 80305, USA
[2]Cooperative Institute for Research in Environmental Sciences, University of Colorado, Boulder, CO 80309, USA

Abstract. This article presents a diode laser-based, cavity ring-down spectrometer for simultaneous in situ measurements of four nitrogen oxide species, NO_3, N_2O_5, NO, NO_2, as well as O_3, designed for deployment on aircraft. The instrument measures NO_3 and NO_2 by optical extinction at 662 nm and 405 nm, respectively; N_2O_5 is measured by thermal conversion to NO_3, while NO and O_3 are measured by chemical conversion to NO_2. The instrument has several advantages over previous instruments developed by our group for measurement of NO_2, NO_3 and N_2O_5 alone, based on a pulsed Nd:YAG and dye laser. First, the use of continuous wave diode lasers reduces the requirements for power and weight and eliminates hazardous materials. Second, detection of NO_2 at 405 nm is more sensitive than our previously reported 532 nm instrument, and does not have a measurable interference from O_3. Third, the instrument includes chemical conversion of NO and O_3 to NO_2 to provide measurements of total NO_x ($= NO + NO_2$) and O_x ($= NO_2 + O_3$) on two separate channels; mixing ratios of NO and O_3 are determined by subtraction of NO_2. Finally, all five species are calibrated against a single standard based on 254 nm O_3 absorption to provide high accuracy. Disadvantages include an increased sensitivity to water vapor on the 662 nm NO_3 and N_2O_5 channels and a modest reduction in sensitivity for these species compared to the pulsed laser instrument. The in-flight detection limit for both NO_3 and N_2O_5 is 3 pptv (2σ, 1 s) and for NO, NO_2 and O_3 is 140, 90, and 120 pptv (2σ, 1 s) respectively. Demonstrated performance of the instrument in a laboratory/ground based environment is better by approximately a factor of 2–3. The NO and NO_2 measurements are less precise than research-grade chemiluminescence instruments. However, the combination of these five species in a single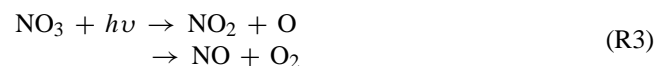 instrument, calibrated to a single analytical standard, provides a complete and accurate picture of nighttime nitrogen oxide chemistry. The instrument performance is demonstrated using data acquired during a recent field campaign in California.

1 Introduction

The nitrate radical, NO_3 and its reservoir species, dinitrogen pentoxide (N_2O_5) are important trace gases in the nocturnal atmosphere (Wayne et al., 1991). NO_3 is formed by reaction of ozone with NO_2 (Reaction R1), and reacts with NO_2 to reversibly form N_2O_5 (Reaction R2).

$$O_3 + NO_2 \rightarrow NO_3 + O_2 \tag{R1}$$

$$NO_3 + NO_2 \leftrightarrows N_2O_5 \tag{R2}$$

These species are typically present at very modest levels during daytime (less than 1 pptv) because NO_3 undergoes rapid photolysis and reaction with NO, which is present during the day and in close proximity to large NO_x emission sources during the night.

$$\begin{aligned} NO_3 + h\upsilon &\rightarrow NO_2 + O \\ &\rightarrow NO + O_2 \end{aligned} \tag{R3}$$

$$NO_3 + NO \rightarrow 2\,NO_2 \tag{R4}$$

The nitrate radical is a strong oxidant and is consumed by reactions with biogenic VOCs and sulfur compounds, and some classes of highly reactive anthropogenic VOCs (Atkinson, 1991). N_2O_5 undergoes heterogeneous uptake to aerosol. Its hydrolysis leads either to non-photochemical conversion of NO_x to soluble nitrate via production of HNO_3 (Jones and Seinfeld, 1983), or to activation of photolabile halogens through formation of nitryl chloride, $ClNO_2$ (Finlayson-Pitts et al., 1989; Thornton et al., 2010). Thus,

NO$_3$ and N$_2$O$_5$ are intermediates in a number of important atmospheric chemical transformations, and understanding their atmospheric concentrations is an important topic of current research.

Much of the prior database for understanding these processes was based on measurements of NO$_3$ by differential optical absorption spectroscopy (DOAS) over a long, open path or by passive techniques using natural light sources (Platt et al., 1980; Solomon et al., 1989; Plane and Nien, 1992). Such measurements have been extremely useful in developing an understanding of the factors that govern nighttime chemistry. In situ instruments add to this database by enabling measurements from mobile platforms, such as aircraft and ships (e.g., Brown et al., 2007a), and from tall towers (e.g., Brown et al., 2007b). The in situ measurements are valuable for characterizing the strong vertical gradients characteristic of the nocturnal boundary layer or for measurements within the residual daytime boundary layer.

Cavity ring-down spectroscopy (CRDS) is a sensitive technique for in situ measurement of atmospheric trace gases (Brown, 2003). In situ measurement of NO$_3$ was first developed approximately a decade ago and was based on CRDS with either a pulsed dye laser (Brown et al., 2002) or extended cavity diode laser (King et al., 2000). Thermal conversion of N$_2$O$_5$ to NO$_3$ in a second channel enabled direct measurement of the sum of the two compounds and measurement of N$_2$O$_5$ itself by difference. This development ultimately led to the deployment of a CRDS instrument for NO$_3$ and N$_2$O$_5$ on aircraft (Dubé et al., 2006). Although the pulsed laser system used in this instrument had a relatively small footprint, such laser systems are in general somewhat cumbersome for field instruments because of their requirements for power and weight (30 kg and 0.5 kW). In addition, the use of toxic dyes and solvents requires hazardous materials that are not ideal for field environments, especially aircraft.

The aircraft instrument described above also incorporated measurements of NO$_2$ by pulsed laser CRDS at 532 nm by taking advantage of the Nd:YAG laser second harmonic that was used to pump the dye laser (Osthoff et al., 2006). These NO$_2$ measurements required active subtraction of an interference from ozone, but were otherwise accurate (Fuchs et al., 2010). These CRDS NO$_2$ measurements have recently been further developed using a diode laser with a center wavelength near 405 nm (Fuchs et al., 2009). Because there is no significant interference from ozone at this wavelength, this approach is capable of simultaneous detection of NO via its conversion to NO$_2$ in excess ozone. We have also recently demonstrated the analogous conversion of O$_3$ to NO$_2$ in excess NO (Washenfelder et al., 2011).

In this paper, we describe a single CRDS instrument based on diode lasers that measures NO$_3$, N$_2$O$_5$, NO, NO$_2$, and O$_3$. Unlike the previous instruments from our group, this instrument uses a diode laser near the maximum in the NO$_3$ absorption spectrum at 662 nm for the measurement of NO$_3$

and N$_2$O$_5$ (Dubé et al., 2006). This is advantageous in terms of size, weight, power consumption, and elimination of toxic dyes. The main disadvantage to this approach is its increased sensitivity to water vapor. Implications of the water vapor sensitivity for aircraft measurements are described further below. A second diode laser centered near 405 nm is used for detection of NO$_2$ by CRDS and of NO and O$_3$ by chemical conversion to NO$_2$. The NO$_2$ channel provides not only a direct measurement of this compound, but also a method for calibrating the NO$_3$ and N$_2$O$_5$ measurements via the conversion of these compounds to NO$_2$ in excess NO as described by Fuchs et al. (2009). The NO$_2$ measurement is itself calibrated against a standard based on ultraviolet absorption of ozone at 254 nm as described by Washenfelder et al. (2011), providing a common analytical standard for all five species measured by this instrument.

The combination of these five trace gases provides a complete picture of the nighttime chemistry shown in Reactions (R1)–(R4). Measurements of NO$_2$ and O$_3$ provide the source for NO$_3$ formation. Direct measurement of NO$_3$ and N$_2$O$_5$ allow for understanding of their chemistry in the nighttime atmosphere. Measurement of NO characterizes the most important nighttime sink for NO$_3$ in near source regions (e.g., low altitude over urban areas). This paper describes the design and operation of this instrument, and its deployment on aircraft.

2 Instrument description

CRDS is commonly used for sensitive detection of trace gases and has been described in several reviews (Busch and Busch, 1999; Brown, 2003; Atkinson, 2003). CRDS is a direct absorption spectroscopy in which the optical path length is enhanced by a high finesse cavity formed by a set of two highly reflective mirrors. A laser is directed into the cavity, the optical intensity builds in the cavity, and then the laser is turned off quickly compared with the decay of optical intensity in the cavity. The exponential decay of light intensity from the cavity is monitored by measuring the light transmitted through the back mirror. When an absorber is present, the exponential decay time constant is reduced, providing an absolute measurement of optical extinction, as given in Eq. (1).

$$\sigma[\text{A}] = \alpha = \frac{R_1}{c}\left(\frac{1}{\tau} - \frac{1}{\tau_0}\right) \tag{1}$$

Here, σ is the absorption cross-section corresponding to the absorber, averaged under the spectrum of the laser, [A] is the concentration of the absorber, α is the optical extinction coefficient (units of inverse length), c is the speed of light, τ and τ_0 are the exponential decay constants with and without the absorber in the cavity and R_1 is the ratio of the total length of the cavity to the length over which the absorber is present.

The instrument described here consists of two largely independent parts that share a common set of electronics, data
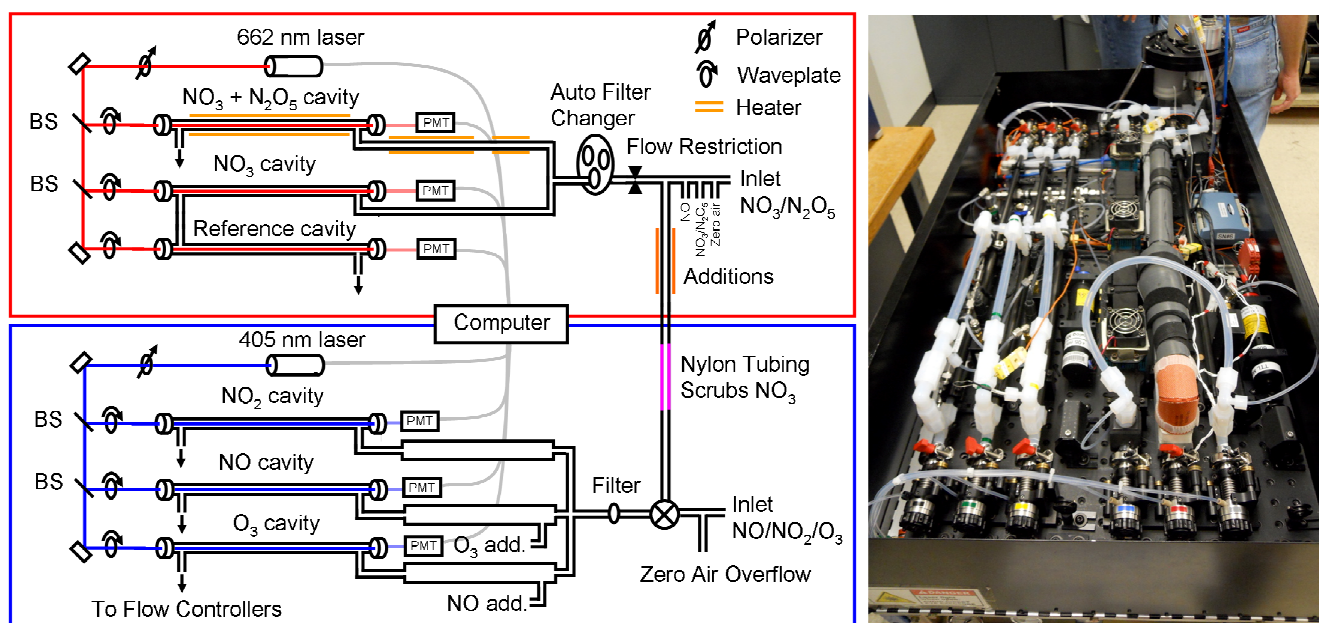
Fig. 1. Instrument schematic. The upper part framed in red shows the NO$_3$ and N$_2$O$_5$ measurement. The lower part framed in blue shows the NO, NO$_2$ and O$_3$ measurement. BS denotes a beamsplitter. A photo of the optical bench instrument is shown on the right.

acquisition, frame and optical mounting system. The first part is the measurement of NO$_3$ and N$_2$O$_5$ using a 662 nm diode laser. The second is the measurement of NO$_2$, NO, and O$_3$ using an additional 405 nm diode laser. The two parts of the instrument have separate inlets that are only connected together during automated calibrations, as described further below. A schematic of the instrument is shown in Fig. 1 with NO$_3$/N$_2$O$_5$ measurement framed in red and the NO/NO$_2$/O$_3$ measurement framed in blue. A photo of the instrument is shown in the right panel of Fig. 1.

2.1 NO$_3$ and N$_2$O$_5$ measurement

Previous NO$_3$ and N$_2$O$_5$ instruments from our group were based on cavity ring-down spectroscopy using a pulsed dye laser and a Nd:YAG laser to pump the dye laser. Diode lasers, which are available at wavelengths near the 662 nm absorption maximum of the nitrate radical, are a suitable alternative that are smaller, lighter, lower in power consumption and do not require hazardous material. Like pulsed dye lasers, commercially available Fabry-Perot diode lasers are spectrally broad enough to couple passively to the mode structure of the optical cavity (Fuchs et al., 2009). They are also spectrally narrow enough to provide a specific measurement for the nitrate radical. Ayers et al. (2005) and Schuster et al. (2009) have already demonstrated the use of similar diode lasers for detection of NO$_3$ and N$_2$O$_5$. The instrument described here is similar to these instruments aside from two distinct differences. First, our instrument uses an on-axis rather than an off-axis alignment to couple the laser to the optical cavity,

similar to our 405 nm NO$_2$ detection scheme (Fuchs et al., 2009). Since the nominal 0.5 nm width of the diode laser spectrum overlaps more than 2000 longitudinal modes of the 93 cm cavities, it couples passively without active control of the laser spectrum or cavity modes. On-axis coupling also allows for a more compact (i.e., smaller diameter) sample cell, decreasing sample residence time and simplifying the optical alignment. Second, this instrument incorporates an automated calibration for NO$_3$ and N$_2$O$_5$ against the NO$_2$ channels.

Light is provided by a continuous wave (cw) diode laser (Power Technology Inc., Fabry-Perot diode model IQμ series), with an output power of approximately 100 mW. The laser can be temperature tuned over a range of 15–33 °C, corresponding to center wavelengths 659.1–662.7 nm, although individual laser diodes typically vary in tuning range. Upon request, the manufacturer selected a diode with tuning range that includes the nitrate radical's absorption peak near 662 nm. The laser spectrum is typically composed of between 2–4 modes of the laser cavity. Each mode is separated by $\sim$0.4 nm and has a width of $\sim$0.3 nm. The intensity in each mode is determined by the temperature of the laser diode. Certain temperatures give output spectra that are dominated by 1, or at most 2, of these 0.3 nm modes. A compact spectrometer (Ocean Optics USB4000) is used to monitor the laser spectrum. The diode temperature is set to maximize the spectral overlap with the nitrate radical's absorption. The laser operates in cw mode and is modulated on and off by a 0–5 volt square wave input. The rise and fall time of the intensity is less than 30 ns, which is rapid on the time scale of

the intensity decay from the optical cavity. The laser is optically isolated from the cavities in this on-axis alignment in order to prevent potentially damaging back reflections from entering the laser. The isolators consist of a single linear polarizer that is placed in front of the laser, and three separate quarter waveplates; one placed directly in front of each cavity. This design ensures that the polarization through the beamsplitters remains linear, so that the polarization sensitivity of the beamsplitters does not degrade the performance of the isolators.

The cavities consist of two 25 mm diameter, 1 m radius of curvature high-reflectivity dielectric mirrors. The mirrors are separated by 93 cm and mounted to an optical breadboard in a custom bellows mount that allows optical alignment and a flexible seal to the sample volume, from which the mirrors themselves are isolated. The cleanliness of the mirrors is maintained by a small purge flow, 25 sccm, of ultrapure air (zero air) over each mirror to separate the mirror surface from the sample flow. Light transmitted through the back mirror of the each cavity is collected by an optical fiber and detected on a photomultiplier tube (PMT) (Hamamatsu HC120-05M). A colored glass filter (Schott RG665) is used immediately before the PMT to reject stray light.

The ring-down traces are digitalized using 14-bit oscilloscope card (National Instruments PCI-6132) at a rate of 2.5×10^6 samples s^{-1}. A digital output of the oscilloscope card is used to modulate the laser intensity normally at 500 Hz, but this can be adjusted to increase the number of ring-down traces acquired or duration of each ring-down trace. The ring-down traces are transferred to a computer over the PCI bus and co-added in lots of 100. The number of ring-down traces in each lot can be adjusted to correspond with the laser modulation frequency and the desired measurement frequency. The co-added ring-down traces are then fit to a single exponential decay. The ring-down traces are fit using the techniques described by Everest and Atkinson (2008). Usually, the digital Fourier transform method is used; however the linear, LRS, and Levenberg-Marquardt methods are also available. When using the linear fitting method, the laser is turned off after every lot of 100 ring-down traces to measure the zero level of the PMTs. During ambient sampling, only the fit parameters are saved and ring-down traces are discarded after fitting.

The upper panel of Fig. 2 shows a co-added ring-down trace acquired while sampling laboratory air at a cell pressure of 504.6 hPa. The $1/e$ time constant for this ring-down trace is 217.98 ± 0.05 μs where the error is the covariance of the fit parameter. The time constant is determined by the combination of Rayleigh scattering losses, mirror reflectivity, and cavity alignment. The mirror reflectivity is 99.999 %, or 10 ppm transmission. The lower panel in Fig. 2 shows the fit residual as a percentage of the ring-down trace. Higher reflectivity mirrors (Advanced Thin Films, Inc.) with $R = 99.9995$ % (5 ppm transmission) have also been used in this instrument and give a ring-down time constant in excess
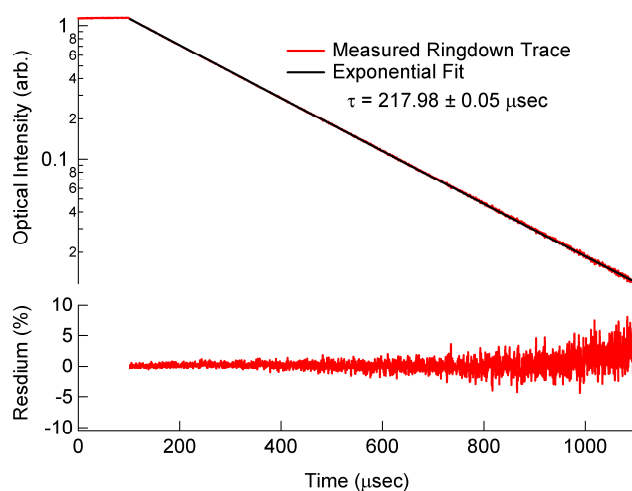
Fig. 2. Upper panel: ring-down trace from one of the 662 nm cavities, along with the fit to the ring-down trace. The lower panel shows the fit residual as a percentage of the fit.

of 400 μs at 500 hPa pressure. All of the performance characteristics described in this paper have been achieved with the lower reflectivity mirrors, which give a larger intensity throughput and allow a higher repetition rate. Instrument performance with the higher reflectivity mirrors is not substantially different. For the lower reflectivity mirrors, the laser is modulated at 500 Hz, and 0.2 s is needed to acquire 100 ring-down traces; thus the overall signal acquisition rate should be 5 Hz. However, due to overhead from transferring ring-down traces to the computer memory, fitting the ring-down traces, and auxiliary measurements, the actual data acquisition rate of the measurement is currently limited to 3 Hz.

The sampling and inlet configuration for NO_3 and N_2O_5 is equivalent to that described by Fuchs et al. (2008) and is described only briefly here. Because NO_3 and N_2O_5 are reactive gases, the inlet is constructed from Teflon tubing and fittings. The shortest possible residence time is needed in order to minimize wall losses for NO_3, which has been shown previously to have a first order loss with respect to reactions on Teflon inlet walls of approximately 0.2 s^{-1} (Dubé et al., 2006).

The inlet consists of several parts and is shown in Fig. 1. The first is a short length of 0.4 cm inner diameter tubing to bring ambient air from outside into the aircraft or instrument enclosure. Following this there are addition points for NO used to determine the instrument zero, zero air used to overflow the inlet, and NO_3/N_2O_5 additions for calibration. Next, a short length of 1.6 mm inner diameter tubing is used as a flow restriction to drop the pressure to approximately half of ambient. A Teflon membrane (Pall Corp. R2PJ047, 2 μm pore size, 25 μm thickness) is used in an automatic filter changer describe by Dubé, et al. (2006) to remove aerosol from the sample flow. After the filter, the flow is split and delivered to each of the two sample cells by 0.64 cm inner

diameter tubing. A 78 cm length of 0.79 cm inner diameter tubing along the axis of each cavity creates the sample cell. Flows are set using flow controllers positioned downstream of the sample cells. One cell remains at ambient temperature to measure the concentration of NO_3. The sample gas in the other channel is heated to convert N_2O_5 to NO_3 in order to detect the sum of NO_3 and N_2O_5. For this channel the gas flow is heated in three stages that are designed to rapidly bring the gas to a temperature sufficient to thermally dissociate N_2O_5 and then to hold it at a temperature where the equilibrium in Reaction (R1) is shifted mainly toward NO_3. For example, the conversion of N_2O_5 to NO_3 based on its equilibrium constant is greater than 98 % for ambient NO_2 levels less than 10 ppbv at 75 °C. The first section is 0.64 cm inner diameter tubing, 40 cm long and held at 130 °C. The second is 25 cm long and held at 80 °C to reduce thermal gradients and minimize flow noise in the sample cell which is held at 75 °C.

A third 662 nm channel is used to continuously monitor the optical extinction from species other than NO_3, such as NO_2, O_3 and water vapor. It consists of an optical cavity and sample cell downstream of the NO_3 sample cell. NO is continuously added to this sample cell in the same manner as the instrument zeroing described below.

The total flow through the inlet is controlled at a constant volumetric flow rate that is adjusted for conditions of a particular measurement campaign. Typical flows for recent aircraft measurements described below were 15 and 9 LPM (liters per minute) for the NO_3 and $NO_3 + N_2O_5$ sample cells, respectively. As in our previously described instrument, the zero for the NO_3 measurement is determined by adding a small amount of NO to the inlet. In an excess of NO, NO_3 is rapidly converted via Reaction (R4) ($k = 2.6 \times 10^{-11}$ cm³ molecule⁻¹ at 298 K) into NO_2, which has an absorption cross-section that is approximately 4×10^4 times smaller than that of NO_3 at 662 nm. This zero method does not influence optical extinction due to ambient levels of O_3, NO_2 or H_2O and is therefore highly specific for NO_3. A small flow of a 100 ppmv NO in N_2 mixture is added to the inlet flow to produce an NO concentration of $\sim 10^{12}$ molecules cm⁻³, designed to give >99.9 % conversion of NO_3 to NO_2 before the flow enters the axis of the NO_3 measurement cell. The zero of the instrument is typically 5 s in duration and is measured at arbitrary intervals depending on requirements. During aircraft ascent and descent, when changes in pressure lead to rapid changes in background time constant due to Rayleigh scattering, the zero interval can be as short as once per minute. On level flight legs or for ground based measurements, a zero interval of 3–5 min is normally sufficient to track any changes in τ_0 due to cavity alignment or variable background absorbers.

2.2 NO, NO₂, and O₃ measurement

Measurement of NO_2 is integral to the NO_3 and N_2O_5 calibrations and measurements of inlet transmission. Measurement of NO_2 using a 405 nm diode laser improves its sensitivity compared to our previously described, 532 nm instrument (Osthoff et al., 2006; Fuchs et al., 2010), since the NO_2 cross-section is approximately 4 × larger at 405 nm. Furthermore, the interference from ozone is essentially eliminated, since its absorption cross-section is approximately 4×10^4 times smaller than that of NO_2 at 405 nm. Both NO and O_3 can be measured by the same instrument via conversion to NO_2; conversion of NO to NO_2 in excess ozone has been described previously by Fuchs et al. (2009), while conversion of O_3 to NO_2 in excess NO has been described by Washenfelder et al. (2011).

A second diode laser centered at 405 nm (Power Technology Inc., Fabry-Perot diode model IQμ series) provides the light source for the CRDS detection of NO_2. Unlike the 662 nm diode laser, this diode laser is not actively temperature tuned and is held at a constant 20 °C. We have found the center wavelength to be stable over the lifetime of the laser by repeated checks against a calibrated grating spectrometer. The laser output power of 80 mW is divided into three equal parts using a 33 % beamsplitter and a 50 % beamsplitter. The three cavities are constructed in the same manner as the 662 nm cavities, except that a bandpass filter centered at 405 nm is used in front of the photomultiplier to reject stray light. The layout is shown schematically in Fig. 1.

The data acquisition for the 405 nm channels is done in the same way as for the 662 nm channels using a second oscilloscope card to modulate the laser and acquire the ring-down down traces. The 405 nm mirrors have a reflectivity of 99.9965 % (35 ppmv transmission) and give typical background time constants of 40 μs at a pressure of 840 hPa. Because the time constants on the 405 nm cavities are shorter than the 662 nm cavities, the laser is modulated at four times the frequency, or 2 kHz. Ring-down traces are acquired in lots of 400 and co-added to achieve the same overall data acquisition rate (3 Hz) as the 662 nm side of the instrument. It is not required that both the 662 nm channels and the 405 nm channels acquire the ring-down traces in lots corresponding to equal acquisition time but doing so maximizes the total number of ring-down traces collected.

The NO, NO_2 and O_3 sample cells have a separate inlet from the NO_3/N_2O_5 measurement, and the inlet is simpler because the 405 nm cavities are operated at ambient pressure and the measured species are less reactive. The inlet and sample cells are constructed with Teflon tubing and fittings. Ambient air is drawn in through a length of 0.4 cm inner diameter tubing to a 1 μm pore size Teflon filter (Pall Corp. R2PL047) in a commercial, PFA Teflon mount (Savillex). The smaller pore-size filter ensures rejection of smaller size aerosol to which the 405 nm channels may in principle be more sensitive. Loss of NO, NO_2 and O_3 on

these filters is negligible. There is no evidence for a signal due to aerosol extinction on the downstream side of these filters during sampling of ambient air. Following the filter, the flow is split into three equal parts and delivered to the sample cells. Before entering each sample cell, there is a reactor consisting of a 33 cm length of 0.95 cm inner diameter tubing. The flow rate through each channel is controlled at 2.7 LPM (volumetric) to maintain a residence time of 0.6 s (plug flow) within each reactor while sampling from variable external pressures from the aircraft. On the first channel which is used for the NO$_2$ measurement, the purpose of the reactor is only to match the residence time of all three channels, so that NO$_2$ may be accurately subtracted from NO$_x$ or O$_x$, as described below.

The second channel measures total NO$_x$ via conversion of NO to NO$_2$ in excess O$_3$. A 12 sccm flow of 0.3 % ozone is added at the beginning of the reactor via a three way valve that allows switching of this ozone addition to a vent line. The ozone is generated by passing a flow of pure oxygen over a mercury-argon lamp (UVP 90-0004-01). The resulting ozone concentration in the sample cell is approximately 4×10^{14} ($\sim$16 ppmv at 1 atmosphere and 298 K) and is measured periodically from the change in optical extinction at 405 nm ($\sim 6 \times 10^{-9}$ cm^{-1}) upon switching the ozone flow into and out of the sample cell. This measurement is checked less frequently using a commercial ozone monitoring instrument. The background extinction due to this added ozone changes the ring-down time constant by approximately 0.25 µs from its nominal value of 40 µs at atmospheric pressure (1013 hPa). The presence of this large excess ozone converts NO quantitatively to NO$_2$ via Reaction (R5).

$$O_3 + NO \rightarrow NO_2 + O_2 \qquad (R5)$$

$$k_{298} = 1.9 \times 10^{-14}\ \text{cm}^{-3}\ \text{molecule}^{-1}\ \text{s}^{-1}$$

Conversion of NO to NO$_2$ under these reactor conditions is greater than 99 %. A small correction of 1–2 % is required to account for the further oxidation of NO$_2$ to higher oxides of nitrogen, NO$_3$ and N$_2$O$_5$, via Reactions (R1) and (R2) (Fuchs et al., 2009). The measured NO$_x$ concentration is also corrected for the small dilution ($\sim$0.5 %) due to the addition of the O$_3$/O$_2$ flow.

The third channel measures total odd oxygen, O$_x$ = NO$_2$ + O$_3$, via the analogous conversion of O$_3$ to NO$_2$ in excess NO. A small flow of NO from a standard mixture of NO in N$_2$ (Scott-Marin) is added at the beginning of the reactor to produce an excess concentration of NO identical to the excess O$_3$ concentration in the NO$_x$ channel (i.e. 4×10^{14} molecules cm^{-3}). The excess NO quantitatively (greater than 99 %) converts O$_3$ in the ambient sample flow to NO$_2$ via Reaction (R5). There is no need for an additional correction for further oxidation of NO$_2$ on this channel since Reactions (R1)–(R2), to the small extent that

they might occur without large, excess O$_3$, are effectively reversed by reaction of NO$_3$ with the excess NO (Reaction R4). The excess NO added to this channel does contain an unavoidable contamination of NO$_2$, which can produce a large background signal. An FeSO$_4$ converter on the outlet of the standard cylinder reduces this NO$_2$ contamination considerably to a background level of 0.5–2 ppbv within the sample cell (Washenfelder et al., 2011).

Maintaining a constant conversion efficiency of O$_3$ and NO to NO$_2$ is a potential challenge for sampling from an aircraft platform since the ambient pressure (and hence the reactant concentration and reactor residence time) is variable with aircraft altitude. Flows on all three 405 nm channels are controlled at constant volumetric rates, rather than constant mass flow rates, to maintain constant residence time and reactant number density in each reactor. Addition of a constant, mass flow of the excess reactant with a well-defined mixing ratio to the variable, volumetric flow produces a constant number density in each reactor as the aircraft ascends and descends. For example, the number density of NO in the O$_x$ sample cell is the product of mixing ratio of the NO standard cylinder (MR), the total number density in the sample cell (N_d) and the ratio of the volumetric flows (F_{NO}^{vol} and F_{cell}^{vol}) as shown in Eq. (2). Here, P is the pressure in the sample cell, P_0 is the standard pressure, k is Boltzmann's constant, T is the sample cell temperature, and F_{NO}^{STD} is the volumetric flow of the reactant at standard pressure and temperature which is directly proportional to the mass flow and independent of pressure.

$$[NO] = MR \times N_d \times \frac{F_{NO}^{vol}}{F_{cell}^{vol}} \qquad (2)$$

$$= MR \times \frac{P}{kT} \times \frac{F_{NO}^{STD}\ (P_0/P)}{F_{cell}^{vol}}$$

Because the flow through the sample cell is maintained at a constant volumetric rate, the only pressure dependences in Eq. (2) are the number density and the reactant volumetric flow, and they cancel each other. The result is a reactant number density that is independent of pressure. Thus, the conversion efficiencies outlined above do not vary with aircraft altitude.

The current scheme for acquiring a zero time constant for the 405 nm channels is identical to that used previously with our 532 nm CRDS NO$_2$ instrument, namely to slightly overflow the inlet with zero air. The overflow is added through a concentric piece of Teflon tubing with an inner diameter slightly larger than the outer diameter of the inlet tubing and which extends slightly (2–4 cm) beyond the inlet tubing. Addition through this concentric inlet minimizes the pressure difference between the zero and signal measurements, which can be significant (1 hPa or greater) if the zero air overflow is added through a simple tee fitting. Such pressure differences between the zero and sample measurement change the

Rayleigh scattering background, which must be corrected for after the measurement. An additional correction is needed to account for the difference in humidity between ambient air and the dry zero air used to overflow the inlet. The difference in the Rayleigh scattering cross-section of water vapor and air was measured at 405 nm by Fuchs et al. (2009) to be 5×10^{-27} cm^2, leading to a maximum correction equivalent to 0.15 ppbv NO$_2$ at 80 % RH (22 °C) . Actual water vapor corrections are typically smaller, however. The potential for an NO$_2$ impurity in the zero air limits the applicability of this zero scheme for sampling in remote environments, where ambient NO$_x$ may be comparable to the NO$_x$ impurity in commercial zero air. Chemiluminescence measurements at our laboratory have found the zero air (Scott-Marin Ultrazero) to have less than 10 pptv of NO$_x$. Zero measurements occurred every 3 min during ambient sampling and lasted 15 s to allow for the zero air to completely fill the sample cell.

The optical extinction due to excess O$_3$ on the NO$_x$ channel, and the NO$_2$ impurity in the added NO on the O$_x$ channel, are not affected by the addition of zero air to the inlet. Thus, no correction is required for these small, background optical extinctions.

3 Calibrations

Although cavity ring-down spectroscopy is, in principle, an absolute method, calibrations are required if either the inlet transmission efficiency for a particular trace gas is not unity, or if the effective absorption cross-section can vary as a function of sampling conditions (i.e., temperature, pressure, laser spectrum). The former is the case for NO$_3$ and N$_2$O$_5$, which are reactive trace gases whose transmission through the inlet system may vary. The latter is potentially the case for NO$_2$ (and by extension, NO and O$_3$ in this instrument) since its absorption cross-section varies with pressure, temperature, and laser spectrum. We have recently developed calibration standards for NO$_3$ and N$_2$O$_5$ based on their conversion to NO$_2$ (Fuchs et al., 2008) and for NO$_2$ based on conversion of standard additions of O$_3$, as described above (Washenfelder et al., 2011). The following sections outline these calibration schemes and their implementation in the current version of this aircraft instrument.

3.1 NO$_2$ calibration

The 405 nm laser diodes provided by the manufacturer vary in center wavelength; hence, the effective cross-section for each laser must be calibrated by standard NO$_2$ additions. Standard concentrations of O$_3$ are generated and measured using a commercial ozone monitor, then quantitatively converted to NO$_2$, which is measured on the CRDS instrument, as described above. The calibrator contains its own NO cylinder and flow controllers for conversion of O$_3$ to NO$_2$
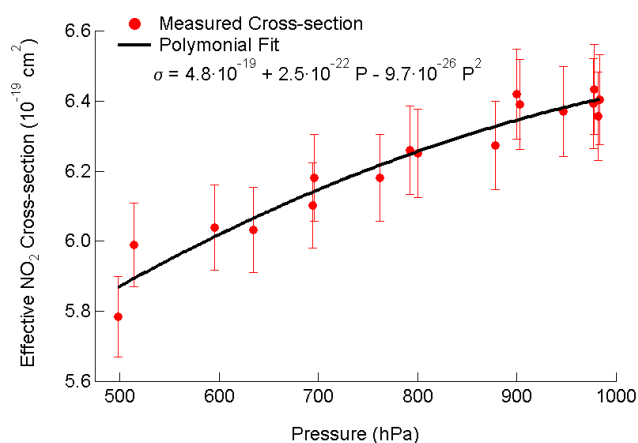
Fig. 3. Pressure dependence of the effective NO$_2$ cross-section at 405 nm. The pressure-dependent cross-section is parameterized by 2nd order polynomial and used for calculating NO$_2$ concentration during aircraft sampling at variable altitudes and cell pressures. The pressure dependence may be due to the variation in the NO$_2$ cross section itself, or to pressure dependence in R_l from Eq. (1). Here, the cross section is fit to a pressure dependence assuming constant R_l of 1.15, though this choice is arbitrary.

such that it delivers standard additions of NO$_2$ independent from the CRDS instrument itself. The calibrator is also field portable and can be used for routine calibration on a daily basis. Typical calibration curves use a series of NO$_2$ mixing ratios between 0–200 ppbv, with the effective NO$_2$ cross-section determined as the slope of a plot of measured optical extinction against NO$_2$ concentration. The effective cross-section is the NO$_2$ cross-section integrated under the laser spectrum and divided by R_l, which is ratio of the cavity length to the length over which the absorber is present.

The cell pressure in the 405 nm channels varies significantly with altitude, typically between 500–900 hPa over the altitude range of the NOAA WP-3 aircraft and is typically 80–100 hPa below ambient pressure. Therefore, any pressure dependence in the effective cross-section for NO$_2$, or in the ratio of the cross section to R_l in Eq. (1), will directly affect the measurement from aircraft. Literature spectra for NO$_2$ do indeed show a pressure dependence (e.g. Vandaele et al., 1998), but only for spectral features too fine to be resolved by the laser system in the CRDS instrument. Nevertheless, the ratio of the effective NO$_2$ absorption cross-section to R_l, i.e., σ/R_l, shows a distinct pressure dependence, as shown in Fig. 3. The value of σ/R_l decreases by approximately 6 % between 1000–500 hPa. The calibration curve in Fig. 3 is the result of multiple determinations in the field on different days, which were reproducible at any given pressure to within ±2 %. For the purpose of calculating the NO$_2$ concentration, the cross-section is parameterized by a 2nd order polynomial. The measured pressure dependence of the effective cross-section may be due to a variation of the actual cross-section or a pressure dependence of R_l. Regardless of
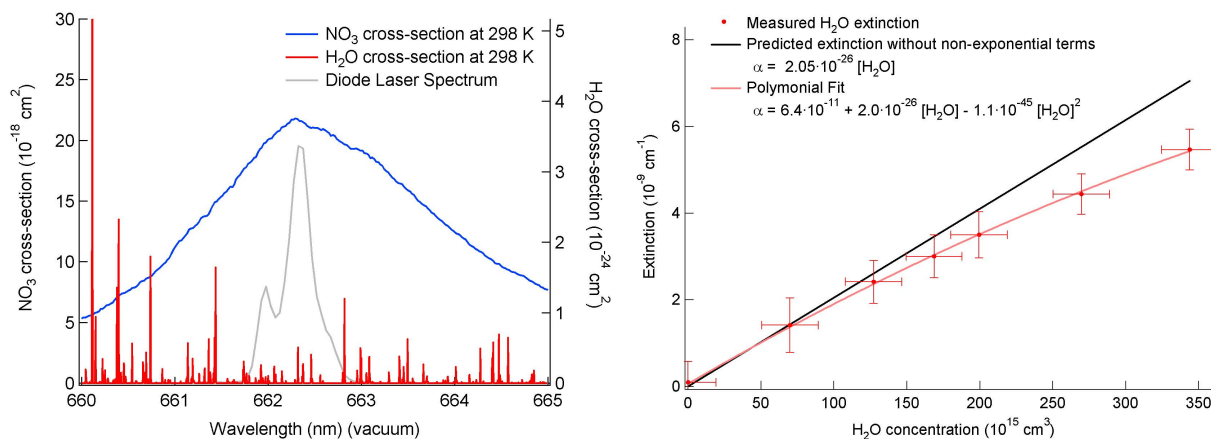
Fig. 4. The right panel shows the NO$_3$ (blue) and water vapor (red) absorption spectrum around 662 nm. A typical laser spectrum is also shown. The left panel shows the measured water sensitivity along with predicted sensitivity neglecting the non-exponential terms. The measured sensitivity is fit to a 2nd order polynomial and used to correct the field data.

the source of the pressure dependence, the effective cross-section is still valid for determination of the NO$_2$ concentration.

3.2 NO$_3$ cross-section and water vapor sensitivity

The cross-section for NO$_3$ is determined using the absorption spectrum measured by Yokelson et al. (1994) shown in Fig. 4 and temperature-dependence determined by Osthoff et al. (2007). Although the absorption spectrum peaks at 2.17×10^{-17} cm^2 for 298 K, the effective cross-section in this instrument is a convolution of the measured cross-section and the laser spectrum and is therefore smaller than the peak absorption. Using a typical laser spectrum shown Fig. 4, the effective cross-section was 2.03×10^{-17} cm^2, a reduction of 7%. One drawback of 662 nm diode laser used in this instrument is that the intensity in different modes, and thus its spectral output, is not stable on the time scale of hours. Based on several measured laser spectra, this instability leads to a variation of 1.5% in the effective NO$_3$ cross-section. The cross-sections measured by Yokelson et al. (1994) and Osthoff et al. (2007) are accurate to ±4%. In this instrument the variability of spectrum increases the inaccuracy of the effective cross-section to ±6%. The laser spectrum is currently measured infrequently (e.g., once per flight) using a small grating spectrometer (Ocean Optics, USB4000) but will be incorporated into routine data acquisition in the future. The NO$_3$ cross-section is temperature dependent, as described previously, such that the effective cross-section for the heated channel is 1.68×10^{-17} cm^2 molecule^{-1} at 348 K.

Water vapor has an absorption in the 662 nm region of the spectrum. The potential for water vapor interference with NO$_3$ measurements is well known from broadband optical measurements of NO$_3$ (e.g. Langridge et al., 2008; Solomon et al., 1989). The water vapor spectrum at 20 °C from the

HITRAN database (Rothman et al., 2009) is shown in red on Fig. 4 along with the nitrate radical absorption spectrum (blue) and typical diode laser spectrum (gray). Our previous, pulsed dye laser instrument had a narrow bandwidth which effectively resolved this water vapor spectrum, and could be tuned off resonance with the discrete water vapor lines while still being tuned effectively to the maximum in the NO$_3$ absorption spectrum. The output of the diode laser, by contrast, unavoidably overlaps multiple water vapor lines, making the instrument much more sensitive to this interference. Furthermore, because the water vapor absorption spectrum consists of several peaks under the laser bandwidth, the variation in absorption cross-section can lead to non-exponential ring-down traces.

The measured sensitivity to water vapor is shown in Fig. 4 (right panel). The extinction is not linear with respect to water concentration because the ring-down transients become slightly non-exponential at higher optical extinctions because of the mismatch between the discrete, water vapor lines and the broadband laser source (Zalicki and Zare, 1995). However, the data can be corrected by using the fitted polynomial as an effective concentration-dependent cross-section as shown in Eq. (3).

$$\tau_{\text{corrected}} = \left(\frac{1}{\tau} + \frac{f([H_2O]) c}{R_l} \right)^{-1} \qquad (3)$$

$\tau_{\text{corrected}}$ is the exponential decay time constant that would be measured in the absence of water vapor. τ is the measured exponential decay constant. $f([H_2O])$ is the fitted polynomial sensitivity and requires an independent measurement of the water vapor mixing ratio. The linear term in the polynomial fit corresponds to the water vapor cross-section when averaged over the laser spectrum and agrees well with the value calculated using the water vapor cross-section obtained from the HITRAN database, 2.05×10^{-26} cm^2. This linear
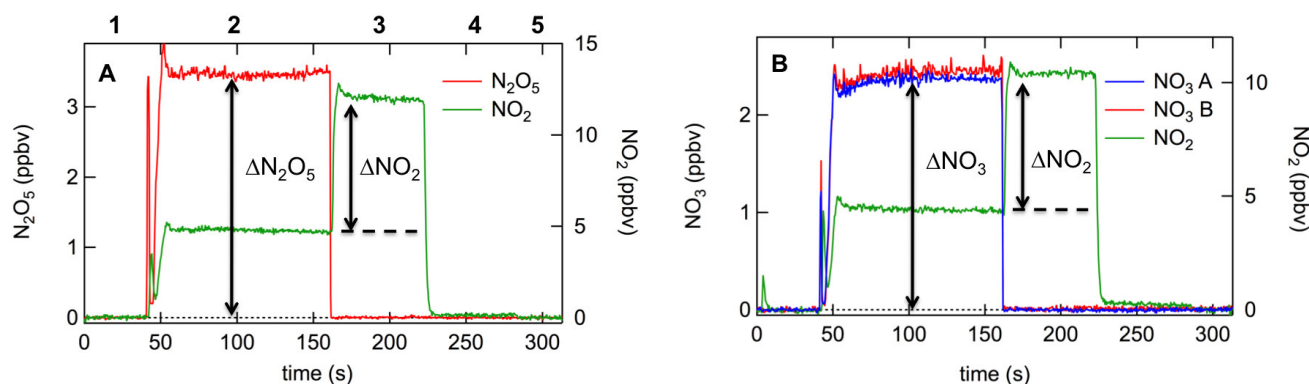
Fig. 5. Example calibration sequences for **(A)** N_2O_5 and **(B)** NO_3. For the N_2O_5 calibration, the N_2O_5 source is added directly to the inlet, while for the NO_3 calibration it first passes through a heater to convert it primarily to NO_3. The sequence of the calibration, indicated by the numbers across the top, includes (1) zero measurement; (2) addition of N_2O_5/NO_3 source; (3) titration of the NO_3/N_2O_5 source with excess NO to convert it to $2 \times NO_2$; (4) N_2O_5/NO_3 source switched off, NO titration on to determine NO_2 content of the added NO; and (5) NO titration turned off. The calibration is given by Eq. (4) and is effectively the ratio of $2 \Delta (N_2O_5)/\Delta NO_2$ (or $2 \Delta NO_3/\Delta NO_2$) marked in the figure, where ΔNO_2 is corrected for the small additional NO_2 in the added NO source given by the difference between Eqs. (4) and (5) in the sequence above. For the data shown in the figure, the N_2O_5 transmission is 99 %. The NO_3 calibrations factors are shown for the ambient channel – NO_3, **(A)** – and the heated channel – NO_3 **(B)**, and are 87 % and 85 %, respectively.

absorption is insensitive to the presence of added NO, and will therefore only interfere with the measurement of NO_3 and N_2O_5 if the water vapor mixing ratio changes rapidly on the time scale of the instrument zero frequency. Such variations can, in principle, be corrected by the reference channel (see above), though in practice the active correction described here proved as useful as a reference channel. For ground based measurements, simple interpolation between zeros would normally be sufficient. However, for aircraft sampling, which may rapidly traverse regions of higher or lower absolute humidity (e.g., on vertical profiles), the interferences must be actively corrected via Eq. (3). A worst-case change in relative humidity of 0 to 100 %, or 3.5×10^{17} cm^{-3} (2.9 % mixing ratio at 20 °C and 505 hPa in the sample cells), would result in an additional extinction of 7×10^{-9} cm^{-1}, or the equivalent of 30 pptv of NO_3/N_2O_5. In practice, we have never observed variations in background extinction that are this extreme; however active correction remains a necessity.

When the water vapor concentration is approximately constant between the zero and the signal measurement, there is an additional, small error due to fitting the slightly non-exponential ring-down transients in the presence of water vapor as though they were single exponentials to retrieve concentrations of NO_3 or N_2O_5. This effect produces a measurement error of less than 0.2 % for either compound.

Although much smaller, both NO_2 and NO_3 have some variation in the cross-section under the laser spectrum like water vapor. We have not observed non-exponential ring-downs from either NO_2 or NO_3. For NO_2 the exponential character of the ring-down trace is further confirmed by the linear extinction as a function of the NO_2 concentration during calibrations.

3.3 NO_3 and N_2O_5 inlet transmission

Wall loss of NO_3 on the Teflon surfaces of the inlet and measurement cells is the most significant source of uncertainty for CRDS measurement of NO_3 and N_2O_5 (Dubé et al., 2006). Characterization of the NO_3 and N_2O_5 transmission efficiency has been described by Fuchs et al. (2008). The following provides a short description of the method and the changes that are specific to the current instrument design. The calibration scheme for NO_3 is based on its chemical conversion to NO_2 with excess NO by Reaction (R4), the same as used for zeroing the 662 nm channels. The resulting NO_2 has negligible inlet loss and can be measured by CRDS at 405 nm to provide a standard for the 662 nm NO_3 measurement. N_2O_5 transmission efficiency can be measured similarly by chemical and thermal conversion of N_2O_5 to NO_2. During transmission efficiency measurement the inlet is overflowed with zero air to avoid interference from ambient O_3 and NO.

Each measurement of NO_3 transmission efficiency has five steps shown in Fig. 5. First, the zero of the instrument is measured as discussed above. Second, the NO_3 source is added to the tip of the NO_3/N_2O_5 inlet and the mixing ratio NO_3 is measured in 662 nm channels. The amount of NO_2 coming from the source directly is measured in the NO_2 channel. As described above, for ambient sampling, the inlet for the NO_2, NO_x and O_x channels is separate from the NO_3 and N_2O_5 inlet; however, during the transmission measurements the NO_2 channel must be connected to the NO_3/N_2O_5 inlet. This connection is made via the three-way valve shown in Fig. 1, which switches the instrument between sampling and calibration mode. Unlike the previously described pulsed laser instrument, in which the NO_3 and NO_2 measurements were

in series, they are in parallel in this instrument, such that measurements of NO_3 or N_2O_5 occur simultaneously with that of NO_2. The third step of the transmission efficiency measurement is to add NO_3 and NO simultaneously to the NO_3/N_2O_5 inlet. The reaction of NO_3 and NO quantitatively converts NO_3 into NO_2 producing two molecules of NO_2 for each molecule of NO_3 added to the inlet. During this step the NO_2 channel measures NO_2 from three sources: NO_2 coming directly from the N_2O_5 calibration source, NO_2 produced by the reaction of NO_3 and NO, and the NO_2 impurity present in the NO addition. The fourth step is to shut off the NO_3/N_2O_5 addition from the calibration source, but leave the NO flow present to measure the NO_2 impurity present in this NO. The fourth step accounts for this contamination. The fifth step is a second zero measurement, with no addition of either NO or NO_3/N_2O_5.

The N_2O_5 transmission efficiency can be measured by a similar five step procedure with the addition of N_2O_5 to the inlet instead of NO_3; however, during the third step a heater is used to convert the N_2O_5 into NO_3 which is then converted to NO_2 by reaction with NO. This heater is along the connection between the NO_3/N_2O_5 inlet and the NO_2 sample cell and is followed by a short section of nylon tubing which acts as an NO_3 scrubber, as described in Fuchs et al. (2008). In this configuration, the scrubber serves to remove NO_3 from the flow produced by thermal decomposition of N_2O_5 when the NO addition is off during step 2, so that the NO_2 channel measures only the NO_2 arising from thermal dissociation of N_2O_5 and not any optical extinction from NO_3. It also prevents recombination of NO_3 with NO_2 in the NO_2 sample cell. (Both the heater and scrubber are necessary for the NO_3 transmission measurement as well, because our source can not produce pure NO_3. It is unavoidably contaminated with N_2O_5.) During addition of NO, all NO_3 produced in the heater between the inlet and the NO_2 sample cell is converted to $2 \times NO_2$, which is not affected by the scrubber.

Calibration samples of N_2O_5 or NO_3 are generated by passing a small flow of zero air over a sample of solid N_2O_5 stored in a trap at $-78\,°C$ (dry ice). The source produces N_2O_5 with less than 2 % NO_3 or, if switched through an additional heater mounted in the calibration box, greater than 90 % NO_3.

The transmission efficiency can be calculated using the measurements taken during each of the five steps. Equation (4) then gives the expression for the transmission efficiency as the ratio between measured NO_3 during step 2 in the 662 nm channel and 1/2 the NO_2 generated from the conversion in Reaction (R4).

$$T_e = \frac{2 \times [NO_3]}{[NO_2]_{source+NO} - [NO_2]_{source} - [NO_2]_{NO}} \quad (4)$$

Here, $[NO_2]_{source+NO}$ is the NO_2 concentration when both the NO_3 and NO are added to the inlet during step 3, and $[NO_2]_{source}$ and $[NO_2]_{NO}$ are the NO_2 concentrations when

the NO_3 and NO are added to the inlet separately, during steps 2 and 4 respectively.

To relate ambient concentrations with those measured in the sample cells, three separate transmission efficiencies are required: (1) the transmission of N_2O_5 through the heated inlet, T_e (N_2O_5), which is the combination of the transmission efficiency for N_2O_5 itself, the conversion efficiency to NO_3, and the transmission of NO_3 through the heated inlet; (2) the transmission of NO_3 through the ambient channel, $T_e^{ambient}$ (NO_3); and (3) the transmission of NO_3 through the heated channel, T_e^{heated} (NO_3) (Dubé et al., 2006; Fuchs et al., 2008). For the NO_3 channel only the inlet transmission of NO_3 is needed to determine the ambient NO_3 concentration, Eq. (5). However, because N_2O_5 is converted to NO_3 in the inlet and consequently lost to the walls, the inlet transmission of both NO_3 and N_2O_5 is needed to calculate the ambient N_2O_5 concentration, Eq. (6).

$$[NO_3]_{amb} = \frac{[NO_3]_{cell}}{T_e^{ambient} (NO_3)} \quad (5)$$

$$[N_2O_5]_{amb} = \frac{([NO_3] + [N_2O_5])_{cell} - T_e^{heated} (NO_3) [NO_3]_{amb}}{T_e (N_2O_5)} \quad (6)$$

$[NO_3]_{amb}$ and $[N_2O_5]_{amb}$ are the ambient concentration of NO_3 and N_2O_5. $[NO_3]_{cell}$ and $([NO_3] + [N_2O_5])_{cell}$ are the concentrations measured in the sample cells.

Figure 5 illustrates the scheme for an example calibration. Panel a shows the N_2O_5 transmission measurement, while panel b shows the NO_3 transmission measurements in both the ambient and heated measurement cells, which is done simultaneously by addition of NO_3 to both channels. In field calibrations during CalNex showed no dependence of NO_3 transmission efficiency on NO_3 mixing ratio over the range 0.3–4.3 ppbv, although calibrations on any given day were normally performed at a single concentration.

4 Detection limits, accuracy, and sample data

Figure 6 shows a representative measurement of the NO_3 and N_2O_5 instrument baseline precision in our laboratory while sampling zero air. The Allan variance plot gives a detection limit under ~1 pptv (2σ) in 1 s for both species. For NO_3, this sensitivity is comparable to, but slightly worse than that reported by Dubé et al. (2006) (e.g., 0.5 pptv, 1 s, 2σ) using the Nd:YAG/dye laser instrument. For N_2O_5, the sensitivity is slightly improved over the pulsed laser version (e.g., 2 pptv, 1 s, 2σ), although the improvement derives more from reduction in the optical noise associated with the fast flow in the heated channel than with any change in the optical system itself. The reduction in precision compared to the previously reported, pulsed laser instrument is due to a combination of factors, including reduced performance from the composite optical bench and cavity ring-down mirrors experience during the CalNex field intensive, and is not due
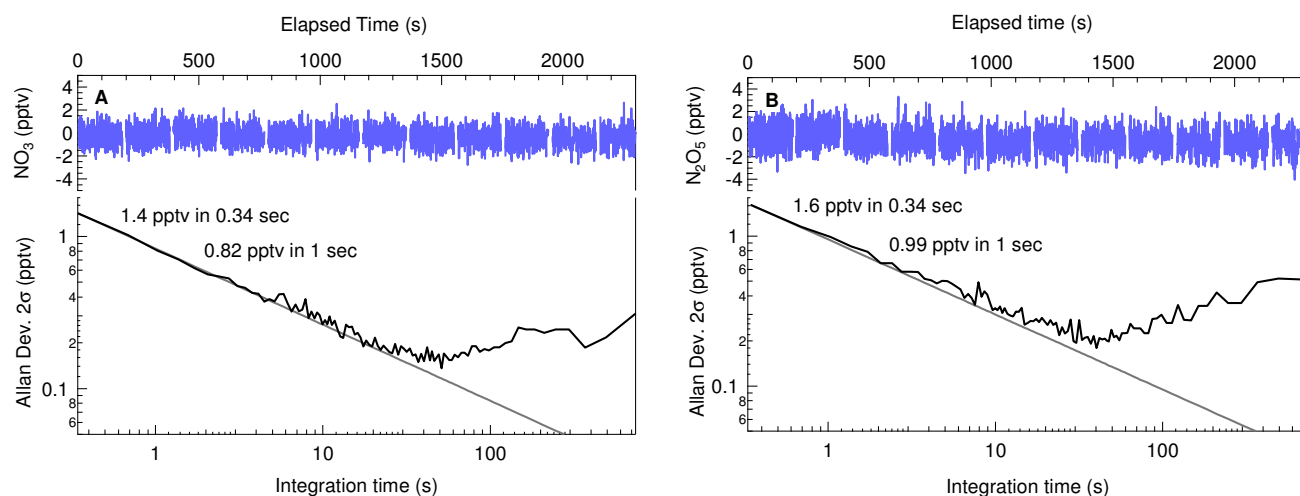
Fig. 6. Allan variance plots for the NO_3 (upper) and N_2O_5 (lower) measurements when sampling synthetic zero air. Both channels have a 2σ precision better than 1 pptv in 1 s.

solely to the introduction of diode lasers. Due to environmental effects (e.g. vibrations on the aircraft) and variations in the ambient air (e.g. temperature gradients), the precision of the instrument is reduced while sampling ambient air in flight. The in-flight detection limits are determined from daytime measurements during CalNex when the ambient mixing ratios of both NO_3 and N_2O_5 were below the laboratory detection limits and were 3 pptv (2σ) in 1 s for both NO_3 and N_2O_5.

The laboratory detection limits for the NO_2 and O_3 measurements have been reported in a separate publications (Washenfelder et al., 2011) and are 46 pptv and 56 pptv (1 s, 2σ) respectively. Our previously reported, ground based NO_x instrument (Fuchs et al., 2009) exhibits a better precision of 22 pptv (2σ, 1 s). In-flight baseline precision can be determined during zero measurements, which are 10–15 s in duration. For NO, NO_2, and O_3 the in-flight detection limits were 140 pptv, 90 pptv, and 120 pptv, respectively. These detection limits are the average precision of 140 zero measurements from an 8 h flight on 3 June 2010. During some time periods, the aircraft measurements of NO, NO_2 and O_3 also suffer from an optical instability in flight that leads to drifts on the order of 0.1–0.3 ppbv in flight. The longer-term baseline instability is most likely related to the mechanical stability of the optical cavity alignments on these channels. Investigation into the source of this instability and potential solutions is ongoing, although it could be addressed by simply increasing the frequency of zero measurements from the current 5 min interval. We anticipate improvements, primarily in the data acquisition software, to improve the precision of the NO_x and O_3 channels on the aircraft instrument.

The accuracy of the NO_3 and N_2O_5 measurements were described in detail by Fuchs et al. (2008), are unchanged by modifications described here. The N_2O_5 accuracy ranges from -8% to $+11\%$ (1σ). The major uncertainties

contributing to the accuracy are uncertainty in the cross-section, R_1, inlet loss and filter aging. Because the filter aging can only decrease the measured mixing ratios, it only contributes to the upper limit of the accuracy. The same factors contribute to the accuracy of the NO_3 measurement (-9%, $+12\%$, 1σ). However, the inlet loss of NO_3 is more uncertain leading to a decreased accuracy compared with N_2O_5.

For measurements of NO, NO_2 and O_3, the accuracy is dominated by uncertainty of the effective cross-section which is directly related to the $\pm 2\%$ accuracy of the UV ozone monitor used to measure the cross-section as describe in section 3.1. There is additional uncertainty ($\pm 1\%$) in the dilution associated with the NO addition required to convert the O_3 to NO_2. The total accuracy for each of three measurements is $\pm 3\%$ (1σ).

This aircraft instrument was deployed during the CalNex campaign in California on the NOAA WP-3 aircraft and took measurements on 25 research flights. An example of the performance and utility of this instrument is shown in Fig. 7, which shows data from a flight in the Los Angeles basin on 3 June 2010. The flight track is shown on the left panel of the figure. This flight includes a series of vertical profiles over the ocean and the urban area of the Los Angeles basin. The flight began in late evening and landed 2 hours after sunrise. The second panel shows the measured NO_3 and N_2O_5 concentrations during the flight along with altitude. The yellow background indicates the solar elevation angle and time of sunrise. The mixing ratios of NO_3 and N_2O_5 vary strongly with altitude, consistent with the previous measurements of vertical stratification within the nighttime atmosphere (Brown et al., 2007a).

The NO, NO_2 and O_3 data for the same flight are shown in the left panels of Fig. 8. Very little NO was encountered during darkness on this flight since the majority of the sampled air masses were distant from direct NO_x emission sources.
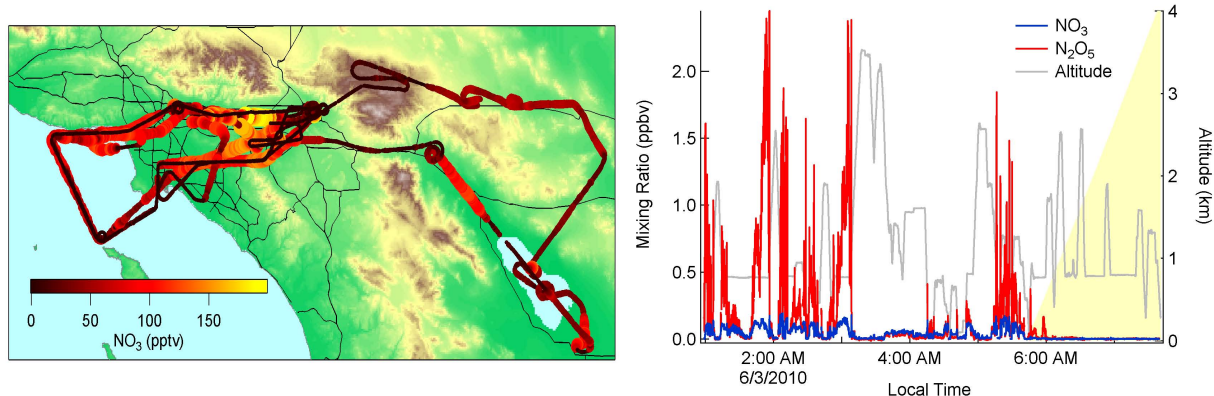
Fig. 7. Sample NO_3 and N_2O_5 data from the flight on 3 June 2010. The left panel shows the flight track in the Los Angeles basin. The right panel shows the NO_3 (blue) and N_2O_5 (red) mixing ratios measured during the flight along with the aircraft altitude in gray. The yellow background indicates the time of sunrise.
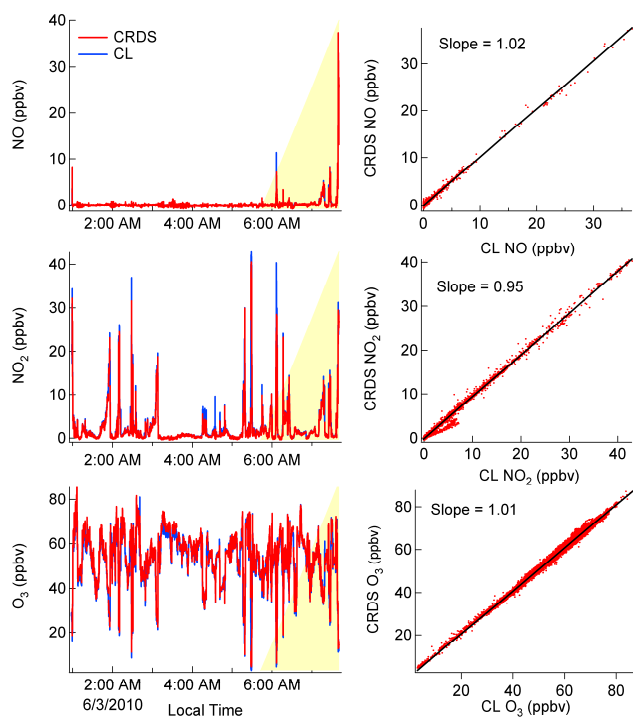
Fig. 8. The left panels show sample NO (upper panels), NO_2 (middle panels) and O_3 (lower panels) mixing ratio from both the CRDS instrument in red and the chemiluminescence (CL) measurements in blue for the 3 June flight. The right panels show the correlations of the two measurements for each species. There was a small population of points on this flight for which there was a deviation on the NO_2 measurement, likely related to the zero measurement on one or the other instruments. These deviations were not observed on other CalNex flights.

Several NO_2 plumes were encountered throughout the night, many of which showed distinct anticorrelations with O_3 due to titration and subsequent nighttime chemistry within these plumes. After sunrise, the NO_x containing plumes showed

measurable levels of NO, which peaked near 30 ppbv during landing at Ontario airport.

The standard P-3 instrument for measurement of ambient NO, NO_2 and O_3 is a custom-built, high-precision, research grade chemiluminescence (CL) instrument (Ryerson et al., 1999, 2000, 2003). The NO_2 channel of the CL instrument has recently undergone substantial improvement to the photolysis system for conversion of NO_2 to NO and modifications of inlet and sample flow path for improved time response of all channels (Pollack et al., 2011). The right three panels of Fig. 8 show the scatter plots comparing NO, NO_2, and O_3 measurements from the 405 nm CRDS instrument with those from the CL instrument at 1 s time resolution. The instruments agree to within 3 % for NO, 5 % for NO_2, and 1 % for O_3 measurements, which is within the summed accuracy of both instruments for each species. Correlation among all measurements was excellent, with R^2 values ≥ 0.99. Much of the scatter in the correlation plots is the result of synchronization between the instruments when transecting NO_x plumes with sharp edges. Although CRDS is lower in precision than the CL instrument and is subject to some baseline instability as described above, the comparisons in Fig. 8 demonstrate that it is accurate, at least at larger NO_x and O_3 values.

One common diagnostic used to understand the nighttime reactivity of NO_3 and N_2O_5 is their steady state atmospheric lifetime (Platt et al., 1984). The steady state lifetime of a species can be determined from its rate of production and its concentration, defined in Eqs. (7) and (8) for NO_3 and N_2O_5(Brown et al., 2003).

$$\tau_{SS}\,(NO_3) = \frac{[NO_3]}{k_1\,[O_3]\,[NO_2]} \approx \left(k_{NO_3} + k_{N_2O_5}\,K_{eq}\,[NO_2]\right)^{-1} \quad (7)$$

$$\tau_{SS}\,(N_2O_5) = \frac{[N_2O_5]}{k_1\,[O_3]\,[NO_2]} \approx \left(k_{N_2O_5} + \frac{k_{NO_3}}{K_{eq}\,[NO_2]}\right)^{-1} \quad (8)$$

Here $\tau_{SS}\,(NO_3)$ and $\tau_{SS}\,(N_2O_5)$ are the steady state lifetimes and $k_1$is the rate constant for Reaction (R1). When the steady
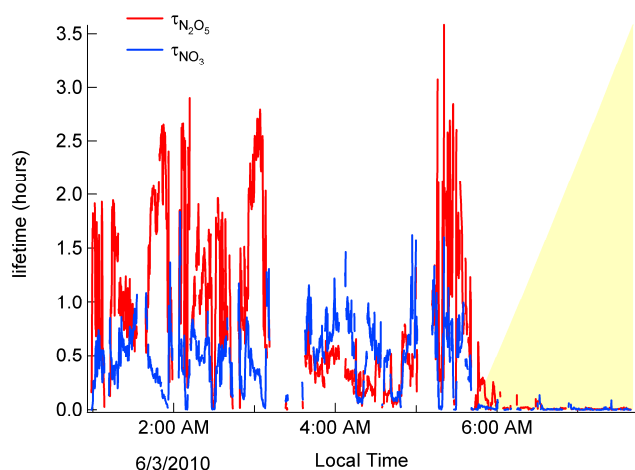
Fig. 9. The lifetimes of NO_3 (blue) and N_2O_5 (red) for the 3 June flight. The lifetimes were calculated using concentrations measured by a single instrument.

state approximation is valid the lifetimes can be used to determine the pseudo first-order loss rate of NO_3 and N_2O_5, k_{NO_3} and $k_{N_2O_5}$. K_{eq} is the equilibrium constant for Reaction (R2). In past field campaigns, this analysis would require data from at least two separate instruments. Figure 8 demonstrates the advantage of the combined measurements of nighttime nitrogen oxides (NO_2, NO_3 and N_2O_5) and O_3 into a single instrument. Figure 9 shows the steady state lifetimes for the flight of 30 May. The lifetimes of NO_3 range from 0–1.5 h and lifetimes up to 3 h are observed for N_2O_5. Thus, the combination of NO_2, O_3 with NO_3 and N_2O_5, all tied to a single analytical standard, provides a complete and accurate representation of nighttime nitrogen oxide chemistry.

5   Conclusions

The article has described an aircraft instrument for atmospheric measurements of NO_3, N_2O_5, NO, NO_2, and O_3 by cavity ring-down spectroscopy. NO_3 and NO_2 are measured directly using a diode lasers with center wavelengths of 662 nm and 405 nm. N_2O_5 is thermally converted to NO_3 for measurement and NO and O_3 are chemically converted to NO_2 and measured. Each channel is regularly calibrated in the field by a scheme linking the cross-sections of each measured species to the O_3 cross-section at 254 nm. The inlet transmission of NO_3 and N_2O_5 is also measured regularly in the field. The performance of the instrument was demonstrated during its first deployment on the NOAA P-3 in California during a 2010 field intensive.

Edited by: W. R. Simpson

References

Atkinson, D. B.: Solving chemical problems of environmental importance using cavity ring-down spectroscopy, Analyst, 128, 117–125, doi:10.1039/b206699h, 2003.

Atkinson, R.: Kinetics and mechanisms of the gas-phase reactions of the NO_3 radical with organic-compounds, J. Phys. Chem. Ref. Data, 20, 459–507, 1991.

Ayers, J. D., Apodaca, L., Simpson, W. R., and Baer, D. S.: Off-axis cavity ring-down spectroscopy: Application to atmospheric nitrate radical detection, Appl. Optics, 44, 7239–7242, 2005.

Brown, S. S.: Absorption spectroscopy in high-finesse cavities for atmospheric studies, Chem. Rev., 103, 5219–5238, doi:10.1021/cr020645c, 2003.

Brown, S. S., Stark, H., Ciciora, S. J., McLaughlin, R. J., and Ravishankara, A. R.: Simultaneous in situ detection of atmospheric NO_3 and N_2O_5 via cavity ring-down spectroscopy, Rev. Sci. Instrum., 73, 3291–3301, doi:10.1063/1.1499214, 2002.

Brown, S. S., Stark, H., and Ravishankara, A. R.: Applicability of the steady state approximation to the interpretation of atmospheric observations of NO_3 and N_2O_5, J. Geophys. Res.-Atmos., 108, 5219–5238, doi:10.1029/2003jd003407, 2003.

Brown, S. S., Dubé, W. P., Osthoff, H. D., Stutz, J., Ryerson, T. B., Wollny, A. G., Brock, C. A., Warneke, C., de Gouw, J. A., Atlas, E., Neuman, J. A., Holloway, J. S., Lerner, B. M., Williams, E. J., Kuster, W. C., Goldan, P. D., Angevine, W. M., Trainer, M., Fehsenfeld, F. C., and Ravishankara, A. R.: Vertical profiles in NO_3 and N_2O_5 measured from an aircraft: Results from the NOAA P-3 and surface platforms during NEAQS 2004, J. Geophys. Res., 112, D22304, doi:10.1029/2007JD008883, 2007a.

Brown, S. S., Dubé, W. P., Osthoff, H. D., Wolfe, D. E., Angevine, W. M., and Ravishankara, A. R.: High resolution vertical distributions of NO_3 and N_2O_5 through the nocturnal boundary layer, Atmos. Chem. Phys., 7, 139–149, doi:10.5194/acp-7-139-2007, 2007b.

Busch, K. W. and Busch, M. A.: Cavity-ringdown spectroscopy, American Chemical Society, Washington, DC, 1999.

Dubé, W. P., Brown, S. S., Osthoff, H. D., Nunley, M. R., Ciciora, S. J., Paris, M. W., McLaughlin, R. J., and Ravishankara, A. R.: Aircraft instrument for simultaneous, in situ measurement of NO_3 and N_2O_5 via pulsed cavity ring-down spectroscopy, Rev. Sci. Instrum., 77, 034101, doi:10.1063/1.2176058, 2006.

Everest, M. A. and Atkinson, D. B.: Discrete sums for the rapid determination of exponential decay constants, Rev. Sci. Instrum., 79, 023108, doi:10.1063/1.2839918, 2008.

Finlayson-Pitts, B. J., Ezell, M. J., and Pitts, J. N.: Formation of chemically active chlorine compounds by reactions of atmospheric NaCl particles with gaseous N_2O_5 and $ClONO_2$, Nature, 337, 241–244, 1989.

Fuchs, H., Dubé, W. P., Ciciora, S. J., and Brown, S. S.: Determination of inlet transmission and conversion efficiencies for in situ measurements of the nocturnal nitrogen oxides, NO_3, N_2O_5 and NO_2, via pulsed cavity ring-down spectroscopy, Anal. Chem., 80, 6010–6017, doi:10.1021/ac8007253, 2008.

Fuchs, H., Dubé, W. P., Lerner, B. M., Wagner, N. L., Williams, E. J., and Brown, S. S.: A sensitive and versatile detector for atmospheric NO_2 and NO_x based on blue diode laser cavity ring-down spectroscopy, Environ. Sci. Technol., 43, 7831–7836, 2009.

Fuchs, H., Ball, S. M., Bohn, B., Brauers, T., Cohen, R. C., Dorn, H.-P., Dubé, W. P., Fry, J. L., Häseler, R., Heitmann, U., Jones, R. L., Kleffmann, J., Mentel, T. F., Müsgen, P., Rohrer, F., Rollins, A. W., Ruth, A. A., Kiendler-Scharr, A., Schlosser, E., Shillings, A. J. L., Tillmann, R., Varma, R. M., Venables, D. S., Villena Tapia, G., Wahner, A., Wegener, R., Wooldridge, P. J., and Brown, S. S.: Intercomparison of measurements of NO_2 concentrations in the atmosphere simulation chamber SAPHIR during the NO3Comp campaign, Atmos. Meas. Tech., 3, 21–37, doi:10.5194/amt-3-21-2010, 2010.

Jones, C. L. and Seinfeld, J. H.: The oxidation of NO_2 to nitrate – day and night, Atmos. Environ., 17, 2370–2373, 1983.

King, M. D., Dick, E. M., and Simpson, W. R.: A new method for the atmospheric detection of the nitrate radical (NO_3), Atmos. Environ., 34, 685–688, 2000.

Langridge, J. M., Ball, S. M., Shillings, A. J., and Jones, R. L.: A broadband absorption spectrometer using light emitting diodes for ultrasensitive, in situ trace gas detection, Rev. Sci. Instrum., 79, 123110, doi:10.1063/1.3046282, 2008.

Osthoff, H. D., Brown, S. S., Ryerson, T. B., Fortin, T. J., Lerner, B. M., Williams, E. J., Pettersson, A., Baynard, T., Dube, W. P., Ciciora, S. J., and Ravishankara, A. R.: Measurement of atmospheric NO_2 by pulsed cavity ring-down spectroscopy, J. Geophys. Res., 111, D12305, doi:10.1029/2005JD006942, 2006.

Osthoff, H. D., Pilling, M. J., Ravishankara, A. R., and Brown, S. S.: Temperature dependence of the NO_3 absorption cross section above 298 K and determination of the equilibrium constant for $NO_3 + NO_2 - N_2O_5$ at atmospherically relevant conditions, Phys. Chem. Chem. Phys., 9, 5785–5793, doi:10.1039/b709193a, 2007.

Plane, J. M. C. and Nien, C. F.: Differential optical-absorption spectrometer for measuring atmospheric trace gases, Rev. Sci. Instrum., 63, 1867–1876, 1992.

Platt, U., Perner, D., Winer, A. M., Harris, G. W., and Pitts, J. N.: Detection of NO_3 in the polluted troposphere by differential optical-absorption, Geophys. Res. Lett., 7, 89–92, 1980.

Platt, U. F., Winer, A. M., Bierman, H. W., Atkinson, R., and Pitts Jr., J. N.: Measurement of nitrate radical concentrations in continental air, Environ. Sci. Technol., 18, 365–369, 1984.

Pollack, I. B., Lerner, B. M., and Ryerson, T. B.: Evaluation of ultraviolet light-emitting diodes for detection of atmospheric NO_2 by photolysis - chemiluminescence, J. Atmos. Chem., 65(2–3), 111–125, doi:10.1007/s10874-011-9184-3, 2011.

Rothman, L. S., Gordon, I. E., Barbe, A., Benner, D. C., Bernath, P. E., Birk, M., Boudon, V., Brown, L. R., Campargue, A., Champion, J. P., Chance, K., Coudert, L. H., Dana, V., Devi, V. M., Fally, S., Flaud, J. M., Gamache, R. R., Goldman, A., Jacquemart, D., Kleiner, I., Lacome, N., Lafferty, W. J., Mandin, J. Y., Massie, S. T., Mikhailenko, S. N., Miller, C. E., Moazzen-Ahmadi, N., Naumenko, O. V., Nikitin, A. V., Orphal, J., Perevalov, V. I., Perrin, A., Predoi-Cross, A., Rinsland, C. P., Rotger, M., Simeckova, M., Smith, M. A. H., Sung, K., Tashkun, S. A., Tennyson, J., Toth, R. A., Vandaele, A. C., and Vander Auwera, J.: The HITRAN 2008 molecular spectroscopic database, J. Quant. Spectrosc. Ra., 110, 533–572, doi:10.1016/j.jqsrt.2009.02.013, 2009.

Ryerson, T. B., Huey, L. G., Knapp, K., Neuman, J. A., Parrish, D. D., Sueper, D. T., and Fehsenfeld, F. C.: Design and initial characterization of an inlet for gas-phase NO_y measurements from aircraft, J. Geophys. Res.-Atmos., 104, 5483–5492, 1999.

Ryerson, T. B., Williams, E. J., and Fehsenfeld, F. C.: An efficient photolysis system for fast-response NO_2 measurements, J. Geophys. Res.-Atmos., 105, 26447–26461, 2000.

Ryerson, T. B., Trainer, M., Angevine, W. M., Brock, C. A., Dissly, R. W., Fehsenfeld, F. C., Frost, G. J., Goldan, P. D., Holloway, J. S., Hubler, G., Jakoubek, R. O., Kuster, W. C., Neuman, J. A., Nicks Jr., D. K., Parrish, D. D., Roberts, J. M., Sueper, D. T., Atlas, E. L., Donnelly, S. G., Flocke, F., Fried, A., Potter, W. T., Schauffler, S., Stroud, V., Weinheimer, A. J., Wert, B. P., Wiedinmyer, C., Alvarez, R. J., Banta, R. M., Darby, L. S., and Senff, C. J.: Effect of petrochemical industrial emissions of reactive alkenes and NO_x on tropospheric ozone formation in Houston, Texas, J. Geophys. Res., 108, ACH8-1-24, doi:10.1029/2002jd003070, 2003.

Schuster, G., Labazan, I., and Crowley, J. N.: A cavity ring down/cavity enhanced absorption device for measurement of ambient NO_3 and N_2O_5, Atmos. Meas. Tech., 2, 1–13, doi:10.5194/amt-2-1-2009, 2009.

Solomon, S., Miller, H. L., Smith, J. P., Sanders, R. W., Mount, G. H., Schmeltekopf, A. L., and Noxon, J. F.: Atmospheric NO_3 1. Measurement technique and the annual cycle, 40° N, J. Geophys. Res., 94, 11041–11048, 1989.

Thornton, J. A., Kercher, J. P., Riedel, T. P., Wagner, N. L., Cozic, J., Holloway, J. S., Dube, W. P., Wolfe, G. M., Quinn, P. K., Middlebrook, A. M., Alexander, B., and Brown, S. S.: A large atomic chlorine source inferred from mid-continental reactive nitrogen chemistry, Nature, 464, 271–274, doi:10.1038/nature08905, 2010.

Vandaele, A. C., Hermans, C., Simon, P. C., Carleer, M., Colin, R., Fally, S., Merienne, M. F., Jenouvrier, A., and Coquart, B.: Measurements of the NO_2 absorption cross-section from $42\,000\,cm^{-1}$ to $10\,000\,cm^{-1}$ (238–1000 nm) at 220 K and 294 K, J. Quant. Spectrosc. Ra., 59, 171–184, 1998.

Washenfelder, R. A., Dubé, W. P., Wagner, N. L., and Brown, S. S.: Measurement of atmospheric ozone by cavity ring-down spectroscopy, Environ. Sci. Technol., 45, 2938–2944, doi:10.1021/es103340u, 2011.

Wayne, R. P., Barnes, I., Biggs, P., Burrows, J. P., Canosa-Mas, C. E., Hjorth, J., LeBras, G., Moortgat, G. K., Perner, D., Poulet, G., Restelli, G., and Sidebottom, H.: The nitrate radical: Physics, chemistry, and the atmosphere, Atmos. Environ. A-Gen., 25, 1–203, 1991.

Yokelson, R. J., Burkholder, J. B., Fox, R. W., Talukdar, R. K., and Ravishankara, A. R.: Temperature-dependence of the NO_3 absorption-spectrum, J. Phys. Chem., 98, 13144–13150, 1994.

Zalicki, P. and Zare, R. N.: Cavity ring-down spectroscopy for quantitative absorption-measurements, J. Chem. Phys., 102, 2708–2717, 1995.